

# Driving neural oscillations with correlated spatial input and topographic feedback

Axel Hutt,<sup>1,2,\*</sup> Connie Sutherland,<sup>2</sup> and André Longtin<sup>2</sup>

<sup>1</sup>INRIA CR Nancy—Grand Est, CS20101, 54603 Villers-ls-Nancy Cedex, France

<sup>2</sup>Department of Physics, University of Ottawa, 150 Louis Pasteur, Ottawa, Ontario, Canada K1N 6N5

(Received 10 January 2008; revised manuscript received 25 April 2008; published 26 August 2008)

We consider how oscillatory activity in networks of excitable systems depends on spatial correlations of random inputs and the spatial range of feedback coupling. Analysis of a neural field model with topographic delayed recurrent feedback reveals how oscillations in certain frequency bands, including the gamma band, are enhanced by increases in the input correlation length. Further, the enhancement is maximal when this length exceeds the feedback coupling range. Suppression of oscillatory power occurs concomitantly in other bands. These effects depend solely on the ratio of input and feedback length scales. The precise positions of these bands are determined by the synaptic constants and the delays. The results agree with numerical simulations of the model and of a network of stochastic spiking neurons, and are expected for any noise-driven excitable element networks.

DOI: [10.1103/PhysRevE.78.021911](https://doi.org/10.1103/PhysRevE.78.021911)

PACS number(s): 87.19.lj, 02.30.Ks, 02.50.Ey, 87.19.lj

## I. INTRODUCTION

There has been much interest recently in the dynamics of nonlinear systems subjected to spatiotemporal forcing [1]. The interaction of the characteristic length and time scales of the input with those of the system is important for understanding the kinds of patterns that can occur under such forcing, and is still an open question despite significant progress. In some contexts, such as in neural or metabolic networks, this forcing contains information that the system must adequately respond to, often via feedback [2]. Sensory systems, for example, are organized in a feedforward manner, where stimulus information is relayed from primary sensory neurons to higher brain centers, and these in turn feed back to primary areas. This enables patterned responses to specific stimulus features, which the feedback can reinforce or modulate. Of key interest is the induction of patterns in space such as localized bumps [3] or temporal oscillatory behavior [4,5]. There is evidence that oscillations can be important for biasing input selection or enhancing selectivity to stimulus motion [6], altering the connection strength between neurons, and temporarily linking neurons to assemblies [7].

In its simplest form, the receptive field of a given neuron is defined by the feedforward inputs it receives, and thus is made up of all the neurons (and their associated stimulus space) that have an effect on its firing activity. This effect can be excitatory as in the classic center receptive field, or inhibitory, as in the classic inhibitory surround. However, this picture is complicated by feedback pathways in different forms. For example, in the visual system of macaque monkeys, the retina projects in a topographic feedforward manner to the lateral geniculate (LGN), which in turn projects to the primary visual cortex V1. But there are also lateral (“horizontal”) connections within V1. And V1 projects to other areas, which in turn project back to V1 (see, e.g., [8]). These feedback connections shape the classic receptive field and its dependence on stimulus features (such as spatial fre-

quency, orientation tuning, and stimulus contrast), and also mediate long-range effects that modulate the classic receptive field [9,10]. There is debate, for example, as to whether the receptive fields of cells in V1 are significantly determined by fast (short-delay) feedback projections to V1 in conjunction with horizontal connections within V1, rather than by feedforward projection from LGN and horizontal connections within V1. A recent modeling study in fact finds that feedback from higher areas to V1 is a very important determinant of receptive field structure of V1 neurons, and can mediate inhibitory influences in a nontrivial way [11].

Thus the existence of feedback begs an extension of the notion of receptive field or matched filter commonly used to understand how spatial inputs are processed in feedforward networks [12]. Our work considers how such spatially organized feedback affects neural firing activity using an effective receptive field formulation, and focuses closely on oscillatory activity rather than on the genesis of detailed receptive field structure in any particular system. To this end we consider below a system where feedback projections are strong and horizontal connections weak, and are known to mediate oscillations that depend on the spatial structure of the input.

Neural feedback can act globally, or be organized topographically, i.e., locally [13,14] (see Fig. 1) such that a neighborhood of cells projects back near itself via feedback, often after a significant delay. There has been much work on the patterns of activity in recurrent networks (see, e.g., [3,13,15,16]), but little work on their response to spatiotemporal inputs. It is known theoretically that oscillations can be induced in such networks with global delayed feedback when fluctuating inputs to the cells are spatially uniform [17–20], or where each cell receives an adjustable mixture of individual noise and common (global) noise, in agreement with experiment [4,17,21]. These studies focused on global feedback pathways, and thus lack a notion of “neighborhood:” the connections between cells are via global feedback, and the input to each cell is either global or a mixture of global and local noise, i.e., it lacks a clearly defined characteristic length scale. However, little is known about the dynamic role played by topographic feedback pathways which are also known to exist. In particular, their existence

\*axel.hutt@loria.fr

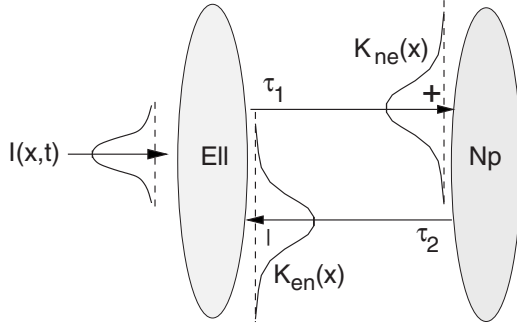


FIG. 1. Topography of the feedback model under study. The plus and minus signs indicate the excitatory and inhibitory connections, respectively. The bell-shaped distributions  $K_{en}(x)$  and  $K_{ne}(x)$  represent the spatial connectivity functions, while the distribution  $I(x, t)$  denotes the spatial correlation function of the external input.

raises the question of how the length scales of feedback interact with the spatial scale of time-varying forcing signals to correlate activity and produce oscillations in excitable systems.

In this work we introduce a model of two neural populations interacting nonlocally via excitatory and inhibitory delayed feedback connections. Thus there are no local horizontal connections within the populations. Further, the topography of feedback connections is studied over a wide range of spatial scales; at the extreme “local” feedback case a neuron essentially feeds back to itself via the other population, while at the global case each neuron affects every other neuron via feedback, as in previous studies [4,17,21]. Moreover, we look at how such local and global delayed feedbacks interact with spatiotemporal noise based on a population rate formulation of the problem, and compare theory to numerics on this model as well as on a realistic network of stochastic spiking neurons.

## II. THE POPULATION RATE MODEL

The model we investigate is grounded in the electrosensory system of electric fish (for anatomical reviews, see [22]), but similar configurations can also be found in parts of the vertebrate brain [23–25], as in many other nonlinear spatial systems. It is made up of two neural populations: (1) the ELL, a layer of pyramidal cells driven by the primary receptors that receive the stimulus, and (2) the higher area Np. These are spatially coupled via feedback, according to normalized connectivity kernels  $K_{en}(x)$  and  $K_{ne}(x)$  denoting connections from the Np( $n$ ) to the ELL( $e$ ) and vice versa, respectively (see Fig. 1). In contrast to these interarea connections, the neurons in both populations have insignificant direct coupling (i.e., horizontal connections), which reflects anatomical findings [22]. Further, the coupling from the ELL to Np is excitatory and delayed in time by  $\tau_1$ , while the coupling back to the ELL is inhibitory [22] with delay  $\tau_2$ . Moreover, the model considers excitatory spatiotemporal stimuli  $I(x, t)$ , which for simplicity are directly relayed to ELL by the receptors.

The present work introduces a model which describes mathematically the mean membrane potential in neural

populations [26,27] and which are strongly related to experimentally observable local field potentials [28,29]. In this description, membrane potentials and firing rates are temporal mean values over a time interval smaller than the typical oscillation period of the systems activity. We focus on how the spatial correlations in the input stimulus interact with those imposed by the topographic feedback to produce network oscillations. Specifically, we will consider below a spatiotemporal noise with a well-defined and adjustable spatial correlation length. We focus on a general scenario where two neural populations interact via feedback; one of them is driven by the spatiotemporal noise, which represents input from another part of the brain, or from a physical stimulus external to the animal (perhaps relayed via primary receptors). We will see how this general case can be replaced by a simpler circuit with self-feedback and a compound connectivity and delay.

The evolution equations read

$$\begin{aligned} \tau_{in} \frac{\partial E(x, t)}{\partial t} &= -E(x, t) + I(x, t) \\ &\quad - g_{in} \int_{\Omega_n} dy K_{en}(x - y) S_n[N(y, t - \tau_2)], \quad (1) \\ \tau_{ex} \frac{\partial N(y, t)}{\partial t} &= -N(y, t) + g_{ex} \int_{\Omega_e} dx K_{ne}(y - x) S_e[E(x, t - \tau_1)], \quad (2) \end{aligned}$$

where  $\Omega_e$  and  $\Omega_n$  are the respective domains of the ELL and the Np; we further assume periodic boundary conditions. Further  $E, N$  and  $S_e, S_n$  denote the mean membrane potential and mean firing rate of principal neurons in ELL and Np, respectively. In addition, the afferent fibers to the Np terminate at excitatory synapses with synaptic efficacy  $g_{ex}$  and response time constant  $\tau_{ex}$ , while the inhibitory synapses of the afferents to the ELL have the synaptic efficacy  $g_{in}$  and the response time constant  $\tau_{in}$ .

To examine the strength of oscillatory activity in the ELL, we assume spatially homogeneous stationary states  $E_0 = \text{const}$ ,  $N_0 = \text{const}$  in the absence of external stimuli [ $I(x, t) = 0$ ] and study small deviations from these states. For sigmoidal firing rate functions, we find a single stationary state that is a solution of  $E_0 = -g_{in} S_n[g_{ex} S_e(E_0)]$ ,  $N_0 = g_{ex} S_e(E_0)$ . This stationary state is interpreted as the resting state of the system, which is perturbed by incoming external inputs. After linearizing Eqs. (1) and (2), and reintroducing the small input  $I(x, t)$  with vanishing spatial and temporal mean, i.e.,  $\langle I(x, t) \rangle = 0$ , we find that the membrane potential deviations in the ELL,  $u(x, t) = E(x, t) - E_0$ , obey

$$\hat{L}u(x, t) = -\frac{g}{\tau_{ex}\tau_{in}} \int_{\Omega_e} dx' F(x - x') u(x', t - \tau_d) + I(x, t) \quad (3)$$

with the nonlinear gain  $g \equiv (\partial S_e / \partial E)(\partial S_n / \partial N) g_{ex} g_{in}$  evaluated at the resting state  $(E_0, N_0)$ , the sum of the time delays  $\tau_d = \tau_1 + \tau_2$ , and the temporal operator  $\hat{L} = \partial^2 / \partial t^2 + (1/\tau_{ex}$

$+1/\tau_{\text{in}})\partial/\partial t + 1/\tau_{\text{ex}}\tau_{\text{in}}$ . Moreover, we find that the system exhibits an effective spatial feedback kernel

$$F(x-x') = \int_{\Omega_n} dy K_{en}(x-y)K_{ne}(y-x'). \quad (4)$$

In other words, the two spatial interactions collapse to a single spatial interaction and the effective spatial feedback kernel is the convolution of the kernels to and from the area  $\text{Np}$ . This kernel, referred to below as the feedback kernel, can be interpreted as a lateral connectivity function of the ELL cells, keeping in mind that these connections are made via another nucleus, and thus involve delays. In the following, the feedback kernel is chosen as the Gaussian distribution  $F(z) = \exp(-z^2/2\sigma_f^2)/\sqrt{2\pi}\sigma_f$  with the standard deviation  $\sigma_f$  representing the spatial extent of the feedback. This choice preserves the total synaptic strength on each neuron irrespective of  $\sigma_f$ . Moreover, the stability of the resting state is given by the complex roots  $\lambda \in \mathcal{C}$  of the characteristic equation  $\tau_{\text{ex}}\tau_{\text{in}}\lambda^2 + (\tau_{\text{ex}} + \tau_{\text{in}})\lambda + 1 + g\tilde{F}(k)\exp(-\lambda\tau_d) = 0$ , where  $\tilde{F}(k)$  is the spatial Fourier transform of the feedback kernel  $F$  and  $k$  denotes the wave number. The root  $\lambda$  is the Lyapunov exponent of (3) and thus the resting state is linearly stable if the real part of  $\lambda$  is negative, i.e.,  $\mathcal{R}(\lambda) < 0$ . In the following we do not study the linear stability in detail but use parameters which guarantee the stability of the resting state.

Now we assume the external input  $I(x, t)$  as a small external perturbation, which maintains the system in the linear regime about the resting state. In the following, we choose  $I(x, t)$  as spatiotemporal noise with

$$\langle I(x, t_1)I(y, t_2) \rangle = Q\delta(t_1 - t_2)C(x - y), \quad (5)$$

with  $C(z) = \exp(-z^2/2\sigma_i^2)/\sqrt{2\pi}$  and where  $Q$  is the noise variance. This means the external stimulus is uncorrelated in time (“white”) and Gaussian correlated in space with correlation length  $\sigma_i$ . Moreover, the intensity of the external input  $\langle I^2(x, t) \rangle$  is a constant independent of  $\sigma_i$ .

### III. THE POWER SPECTRUM

To compute the power spectrum of  $u(x, t)$ , we introduce the Green’s function  $G(x, t)$  by

$$u(x, t) = \int_{\Omega_e} dz \int_{-\infty}^{\infty} dT G(x - z, t - T)I(z, T).$$

Inserting this ansatz into Eq. (3) we gain the expression

$$\hat{L}G(x, t) + s \int_{\Omega_e} dx' F(x')u(x - x', t - \tau_d) = \delta(x, t - \tau_d)$$

with  $s = g/\tau_{\text{ex}}\tau_{\text{in}}$ . The subsequent Fourier transform into the  $k$ - $\omega$  space yields the Fourier transform of  $G(x, t)$  and, consequently, by the back transformation into  $x$ - $t$  space one obtains

$$G(x, t) = \frac{1}{(2\pi)^2} \int_{-\infty}^{\infty} dk \int_{-\infty}^{\infty} d\omega \frac{e^{ikx - i\omega(t - \tau)}}{L(-i\omega) + s\sqrt{2\pi}\tilde{F}(k)\exp(i\omega\tau)}.$$

Then the autocorrelation function  $\langle u^*(x, t_1)u(y, t_2) \rangle$  of the resulting membrane potential can be computed by applying the input correlation function (5) [30]. Here and in the following, the superscript  $*$  denotes the complex conjugate. By virtue of the spatial homogeneity and the temporal stationarity, we find  $\langle u^*(x, t_1)u(y, t_2) \rangle = K(x - y, t_1 - t_2)$  with

$$K(x, t) = \frac{Q}{\sqrt{2\pi}} \int_{-\infty}^{\infty} d\omega \int_{-\infty}^{\infty} dk \bar{C}(k) |\tilde{G}(k, \omega)|^2 e^{i\omega t - ikx}$$

and the Fourier transform of the input correlation function  $\tilde{C}(k)$ . This relation allows us to apply the Wiener-Khinchin theorem [31], i.e., the temporal power spectrum of  $u(x, t)$  is the Fourier transform of the autocorrelation function  $K(0, t)$ . Consequently we obtain the power spectrum of the membrane potential in the ELL,

$$P(\nu, \eta) = Q \int_{-\infty}^{\infty} dl \frac{\tilde{C}(l)}{A(\nu) + B(\nu)\tilde{F}(l) + D\tilde{F}^2(l)} \quad (6)$$

with the frequency  $\nu$ , the function  $A(\nu)$ , the constant  $D$ , and  $B(\nu) = 2s\sqrt{2\pi}[\cos(2\pi\tau)(\alpha\beta - 4\pi^2\nu^2) - 2\pi\nu\sin(2\pi\tau)(\alpha + \beta)]$ . In addition we rescaled space by  $x \rightarrow x/\sigma_i$  and thus  $l = \sigma_i k$  represents the dimensionless wave number. Consequently the Fourier transforms of the feedback kernel  $F(l)$  and the input correlation function  $C(l)$  in dimensionless wave numbers read

$$\tilde{C}(l) = \exp(-l^2/2), \quad \tilde{F}(l) = \exp(-\eta^2 l^2/2). \quad (7)$$

In addition we have introduced  $\eta$  as the ratio of the two characteristic length scales that correlate neural activity in the problem, namely, the feedback spread and the input correlation length, i.e.,  $\eta = \sigma_f/\sigma_i$ . Consequently the relation of the feedback and the input correlation ranges defines the power spectrum in Eq. (6).

To compute the power spectrum numerically, we expanded  $u(x, t)$  into a discrete Fourier basis where the stochastic integral-differential equation (3) is a set of uncoupled stochastic delay differential equations (SDDEs). The spatially correlated input was implemented according to the rules given in [32]. Since each SDDE gives the time evolution of a spatial mode, we integrated each equation separately, Fourier recomposed the obtained solutions to gain  $u(x, t)$ , and computed the temporal power spectrum by a temporal Fourier transform. Figure 2 shows the power spectrum in the ELL for a large, medium, and low value of  $\eta$ . We observe a clear power maximum at about 40 Hz for  $\eta = 1/40$ , i.e., for large input correlations compared to the feedback range, while the larger value  $\eta = 1$  yields a peak at the same frequency with lower power. In contrast, a large value  $\eta = 40$  makes the peak at 40 Hz vanish and leads to a power peak at 0 Hz.

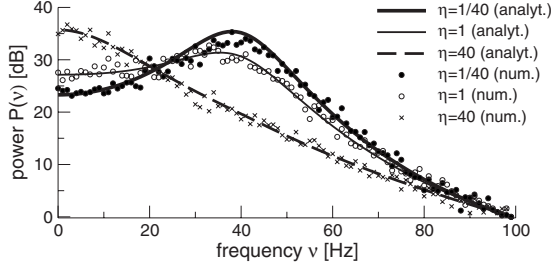


FIG. 2. Power spectrum of the membrane potential  $E$  about the stationary state  $E_0$  for different ratios  $\eta$  of the feedback and the input correlation range. For the numerical simulations, a temporal time step of 0.1 ms and a spatial discretization step of  $5 \mu\text{m}$  with  $10^5$  grid points guaranteed good resolutions in the time domain, the location space, and the  $k$  space. Further parameters are  $\tau_{\text{ex}}=1$  ms,  $\tau_{\text{in}}=8$  ms,  $\tau_d=6$  ms,  $g=1.2$ ,  $Q=0.05$  mV<sup>2</sup>/s, and  $\sigma_f=5$  mm,  $\sigma_i=200$  mm for  $\eta=0.025$ ,  $\sigma_f=\sigma_i=5$  mm for  $\eta=1$ , and  $\sigma_f=200$  mm,  $\sigma_i=5$  mm for  $\eta=40$ . The abbreviations after the  $\eta$  values denote analytical results based on Eq. (6) (analyt.) and numerical results based on Eq. (3) (num.).

To better understand the power peak and its dependence on the relation of feedback and input correlation ranges, we examine the sign of  $dP(\nu, \eta)/d\eta$  for different frequencies and a constant feedback range  $\sigma_f$ . Taking a closer look at the power spectrum in Eq. (6),  $\eta$  occurs in  $\tilde{F}(l)$  only and we find

$$\frac{\partial P(\nu, \eta)}{\partial \eta} = Q \int_{-\infty}^{\infty} dl \frac{2\eta l^2}{2} \underbrace{\frac{\tilde{C}(l)\tilde{F}(l)}{[A(\nu) + B(\nu)\tilde{F}(l) + D\tilde{F}^2(l)]^2}}_{>0} \times [B(\nu) + 2D\tilde{F}(l)]. \quad (8)$$

Since the last term in (8) determines the sign of  $dP(\nu, \eta)/d\eta$ , one can distinguish two cases.

(1) In one case there are some frequencies  $\nu$  for which  $dP(\nu, \eta)/d\eta < 0$ , i.e., the power decreases with increasing  $\eta$  and thus the power increases with increasing input correlation. Equation (8) reveals that this case occurs only if  $B(\nu) < 0$  (necessary condition), i.e., with frequencies in the intervals

$$\nu_m < \nu < \nu_{m+1} \quad \text{with} \quad \tan(2\pi\nu_j\tau_d) = \frac{1 - \alpha\nu_j^2}{\beta\nu_j} \quad (9)$$

and  $m \in \mathbb{Z}_0$ ,  $\nu_m < (1+2m)/4\tau_d < \nu_{m+1}$ ,  $\alpha = 4\pi^2\tau_{\text{ex}}\tau_{\text{in}}$ , and  $\beta = (\tau_{\text{ex}} + \tau_{\text{in}})2\pi$ . In other words, high (low) power for large (small) input correlations is present in frequency bands  $[\nu_0; \nu_1], [\nu_2; \nu_3], \dots$  around  $1/4\tau_d, 5/4\tau_d, \dots$ , and the bandwidths are determined by the total delay time  $\tau_d$  and the synaptic response time constants  $\tau_{\text{ex}}$  and  $\tau_{\text{in}}$ .

(2) In the other case  $dP(\nu, \eta)/d\eta > 0$ , there are some frequencies  $\nu$  at which the power increases with increasing  $\eta$ , i.e., the power increases with decreasing input correlation. From (8) it is obvious that this case occurs for  $B(\nu) > 0$  (sufficient condition) in the complementary frequency bands  $[0; \nu_0], [\nu_1; \nu_2], \dots$

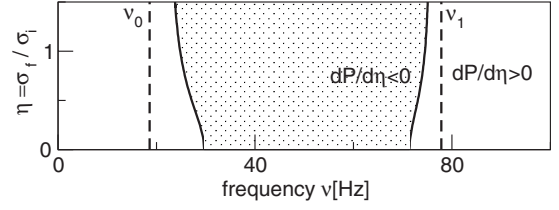


FIG. 3. Frequency bands where the spectral power changes as a function of the ratio  $\eta$ . The dashed vertical lines denote the band borders with frequencies  $\nu_0$  and  $\nu_1$  defined by Eq. (9) while the shaded (nonshaded) area represents the bands of frequencies which exhibit enhanced (attenuated) power upon decreasing  $\eta$ . Further, the solid lines represent the frequency borders obtained numerically from Eq. (6) for  $dP/d\eta=0$ . Other parameters are taken from Fig. 2.

Figure 3 shows the intervals of the necessary condition (9) (dashed lines) and the exact bands computed numerically from Eq. (6) for different values of  $\eta$ . First we observe that the frequency bands defined by (9) are constant with respect to  $\eta$ . They are excellent estimates of the real bands determined numerically from (6), while  $\eta$  slightly changes the numerical borders of the bands. Further, the frequency bands with  $dP/d\eta < 0$  ( $dP/d\eta > 0$ ) at about 40 (0) Hz show good accordance with the band of frequencies in Fig. 2 which exhibits large (small) power for low values of  $\eta$ .

Consequently, the power peak at nonzero frequency in Fig. 2 is defined by the total feedback delay  $\tau_d$ , and the frequency bands of enhanced and attenuated power mainly depend on the feedback delay and the synaptic time constants in the feedback system. Hence the observed frequency bands are rather independent of the external input, as expected from a linearized neural field theory. In contrast, the external input determines the enhancement and attenuation of the oscillations in the frequency bands.

To gain further insight into this mechanism, we can consider the contributions of different factors to the integral that defines the oscillatory power in the time domain  $P(\nu, \eta)$ . Recall the form of the power spectrum  $P(\nu, \eta) = \int_{-\infty}^{\infty} dl R(\nu, l)\tilde{C}(l)$  in Eq. (6). Here  $R(\nu, l)$  represents the response function of the system. The total power thus involves multiplication of the response by the spatial Fourier transform of the noise, followed by an integral over all wave numbers. Figure 4 shows  $R(\nu, l)$  and  $R(\nu, l)\tilde{C}(l)$  for two values of  $\eta$  in the wave number range  $0 \leq l \leq 4$ . For the sake of discussion, we can assume that  $\sigma_f$  was changed, while  $\sigma_i$  remained constant.

In the case of  $\eta=1/40$  [Fig. 4(a)], we find  $\tilde{F}(l) \approx 1$  for this range of wave numbers (not shown). Consequently, we observe a strong system response in the temporal frequency range around  $\nu \approx 40$  Hz, and lower responses away from this range, for all wave numbers shown. Considering the product of  $R(\nu, l)$  and the fast-decaying spatial correlation function  $\tilde{C}(l) = \exp(-l^2/2)$ , which is independent of the frequency [Fig. 4(b)], after integration over all values of  $l$  we find the resulting power peak at about 40 Hz (see Fig. 2).

In contrast,  $\eta=40$  yields a rapidly decreasing function  $\tilde{F}(l)$  with increasing  $l$  and a strong response at low frequencies for all wave numbers, while  $R(\nu, l)$  exhibits similar val-

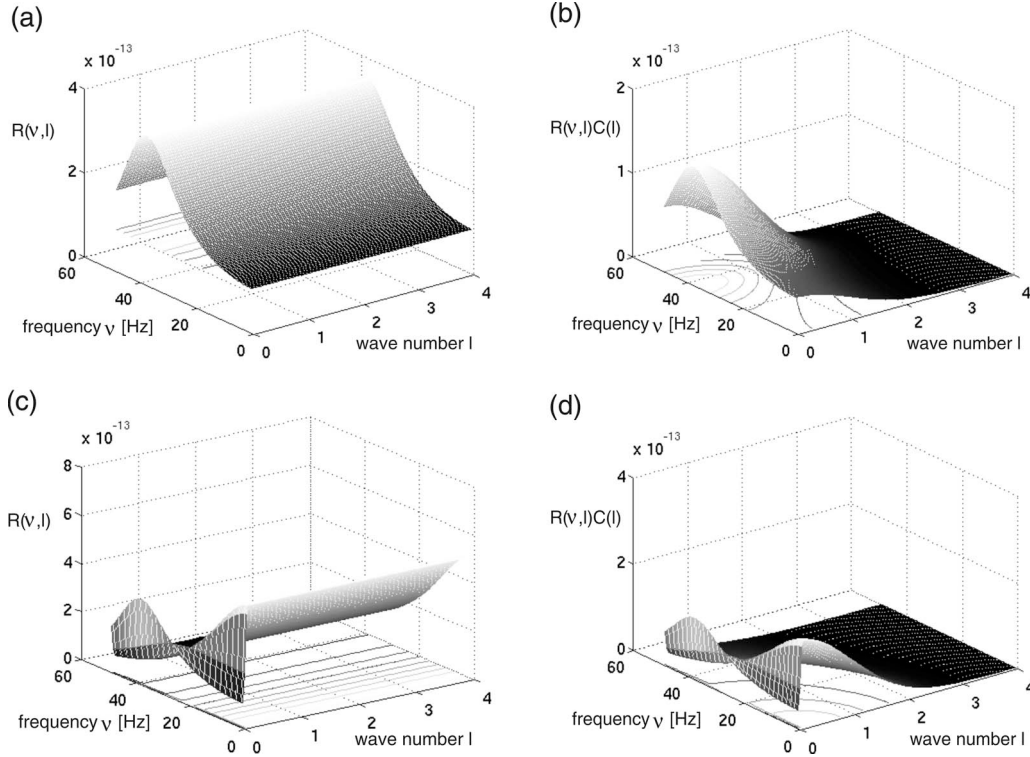


FIG. 4. Response function of the system in Fourier space  $R(\nu, l)$  and the integrand  $R(\nu, l)\tilde{C}(l)$  in Eq. (6) for two values of  $\eta$ =(a), (b)  $1/40$ , and (c), (d)  $40$ . Other parameters are taken from Fig. 2.

ues at  $\sim 40$  Hz for low wave numbers only [Fig. 4(c)]. Consequently the product  $R(\nu, l)\tilde{C}(l)$  exhibits large values at low frequencies for high wave numbers while  $R(\nu, l)\tilde{C}(l)$  shows similar values at  $\sim 40$  Hz for very small  $l$  only [Fig. 4(c)]. Hence integrating  $R(\nu, l)\tilde{C}(l)$  over all  $l$  yields high power values at low frequencies only, outside the gamma range (see Fig. 2).

So we see that the spatiotemporal structure of the feedback system sets up temporal resonances that depend on the wave number. The parameter  $\eta$  determines whether there is one or more resonance along the frequency axis [compare Figs. 4(a) and 4(c)] as well as the range of wave numbers over which the response is relatively strong. A temporal resonance will thus be visible in the time evolution of the system, provided the input noise has sufficient spectral power at lower wave numbers in order to produce a sizable integrand near that resonance. High power at such low wave numbers (longer wavelengths) is seen when the noise is strongly correlated in space—and the difference between “long” and “short” is set by the feedback range, i.e., it is the value of  $\eta$  that counts. The result is that, for a given feedback range, the total power shifts from zero frequency toward frequencies in the gamma range as  $\eta$  decreases. One can see intuitively that, even in the absence of input, the topographic feedback reinforces firing rate oscillations in local neighborhoods because the feedback pulls such neighborhoods together. In the presence of input, local oscillations are further reinforced when a local neighborhood is driven by a coherent noise, which occurs when the input correlation length exceeds the feedback range of connectivity ( $\sigma_i > \sigma_f$ ). The frequency band

around 40 Hz where power increases with  $\eta$  is one that agrees with experimental observations where input correlation produces gamma oscillations in the context of global feedback [4]. The actual frequency range where this effect will be seen depends on the specific parameters of the problem, but qualitatively, it will always be seen. What our results further indicate is that this increase can also occur if the feedback is local rather than global. In this case less input correlation is required to see increased gamma power.

This raises the interesting possibility that a sensory system may detect changes in gamma strength as a function of input parameters, i.e., to signal features of the input such as spatial correlation via strength in the gamma band [33]. One can then ask how much input correlation affects the gamma power. The answer, interestingly, depends only on  $\sigma_f$  and  $\sigma_i$  via their ratio,  $\eta$ , as Fig. 5 reveals. This figure first shows in its left panels that increasing the correlation of the input, i.e., increasing  $1/\eta$ , produces a peak in the gamma range, as in Fig. 2.

Figure 5(c) further plots the integrated power  $\Gamma$  in the gamma range for many different combinations of  $\sigma_f$  and  $\sigma_i$ . Note that changes in  $\sigma_f$  are done by conserving the total synaptic strength onto a given neuron. Further, changes in  $\sigma_i$  are done at constant total stimulus power. When  $\sigma_i$  is small in comparison with the feedback spread, the oscillation is weak. This can change if  $\sigma_i$  increases,  $\sigma_f$  decreases, or both. Opposite behavior occurs in the complementary bands. All results strikingly fall on the same curve predicted by the theory. Significant oscillations arise when  $\sigma_i$  approaches or exceeds  $\sigma_f$ , i.e., when  $\eta$  is  $\sim 1$  or less.

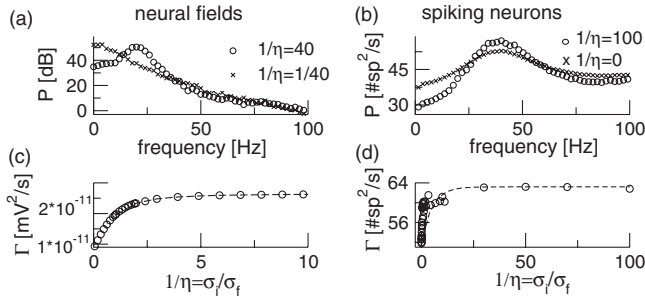


FIG. 5. Comparison of spectral power in neural fields and spiking neuron networks. (a) Power spectra of the neural field for a small ( $1/\eta=1/40$ ) and large ( $1/\eta=40$ ) stimulus correlation length relative to the feedback spread. (b) Power spectra of the spike train from a single stochastic neuron embedded in a network of 100 spiking neurons with topographic delayed feedback for small ( $1/\eta=0$ ) and large ( $1/\eta=100$ ) stimulus correlation length. Each neuron is governed by Eq. (10). (c) Integrated power  $\Gamma$  in the gamma range (30,50) Hz as a function of  $1/\eta$  for the neural field model [Eq. (6)]. (d) Same as (c) except for the spiking neuron network with the power measured in the range (20,40) Hz. The parameters of (a) and (c) are the same as in Fig. 2. The parameters in (b) and (d) are  $\mu=0.5$  (subthreshold regime),  $g=-0.6$ ,  $D=0.08$ ,  $\alpha=3$ ,  $\tau_d=1$ ,  $\tau_r=0.1$ , the spiking threshold is 1, the voltage reset is 0, and all times are in units of the membrane constant, assumed to be 6 ms.

#### IV. THE SPIKING NEURON MODEL

We finally verified our results against simulations of a network of  $N$  stochastic leaky integrate-and-fire (LIF) neurons with delayed spike coupling, as in [17], except that the feedback is no longer global: there is a parameter that specifies the spatial spread of the feedback. Each LIF neuron evolves according to

$$\frac{dV_j}{dt} = -V_j + \mu + \xi_j(t) + I_j(t) + \frac{g}{N} \int_{\tau_d}^{\infty} dt' h(t' - \tau_d) \sum_{k=1}^N F(j-k) x_k(t-t'), \quad (10)$$

where  $V_j$  represents the membrane potential of the  $j$ th neuron in the network,  $\mu$  is the bias (the same for all cells), and each cell receives a time-varying input noise  $I_j(t)$  taken from Eq. (5) with correlation function  $C(j)$ . Further, each neuron has its own internal noise  $\xi_j(t)$  modeled by Gaussian white noise of intensity  $D$ , exhibits a refractory period  $\tau_r$ , and responds to incoming feedback activity by  $h(t) = \alpha^2(t) \exp(-\alpha t)$  with the feedback kernel  $F$  of the neural field model. Here  $x_k$  represents the spike train of the  $k$ th neuron, i.e., a sum of  $\delta$  functions. Similar to the previous model, the feedback delay

is denoted by  $\tau_d$ . This feedback model has been modified from [17] to include the spatial feedback profile  $F(j-k)$ . Figures 5(b) and 5(d) show the same qualitative increase in power in the gamma range as  $\eta$  decreases. We also observe that topographic feedback (large  $1/\eta$ ) enhances gamma activity compared to global feedback (small  $1/\eta$ ). Moreover, for different combinations of  $\sigma_f$  and  $\sigma_i$  the gamma power again falls on a single curve, with a similar qualitative feature as for the neural field model.

#### V. CONCLUSION

In summary, our work describes the influence of a spatiotemporal noise with a well-defined length scale on a delayed negative feedback network. We have shown using theory and numerics that increasing input correlation length can enhance or suppress oscillations in topographic feedback networks with delay. This continues until saturation when the input correlation length  $\sigma_i$  exceeds  $\sigma_f$ , i.e., the effective spatial spread of both feedforward and feedback connections. The topographic feedback enables the system to gauge the spatial correlation of the input by the power in the gamma range. This occurs when the input spatial mode amplitudes are strong and their temporal part is in the gamma range, a condition met when  $\sigma_i \geq \sigma_f$ . This also requires a stimulus temporal bandwidth that encompasses the resonance in the gamma range. We point out that this behavior is a property of both neural field models and spiking networks of stochastic neurons. The former are related to local field potentials (LFPs), while the latter are related to spiking activity, and the equivalence between these two kinds of measurements for various phenomena is a matter of ongoing debate. Recent work reports coherence between LFPs and spiking activity in visual cortex [5] and parietal cortex [34], and our results predict another instance where this equivalence might be observed experimentally.

The synergy between the correlations imposed by spatiotemporal input and those imposed by feedback to produce oscillatory firing activity are general properties of topographic networks, as is the antisynergy in other frequency bands. This complements findings in systems with lateral connections [14,35] where matching input correlation to lateral connectivity causes the highest firing rates. Our results can be generalized to multiple feedback loops, both positive and negative, and can also incorporate the effect of local connectivity, as well as distributions of delays rather than fixed delays.

#### ACKNOWLEDGMENTS

We thank David Hansel for useful discussions. This research was supported by NSERC Canada.

[1] V. K. Vanag, L. Yang, M. Dolnik, A. M. Zhabotinsky, and I. R. Epstein, *Nature (London)* **406**, 389 (2000).  
 [2] J. Bechhoefer, *Rev. Mod. Phys.* **77**, 783 (2005).  
 [3] S. Coombes, *Biol. Cybern.* **93**, 91 (2005).

[4] B. Doiron, M. Chacron, L. Maler, A. Longtin, and J. Bastian, *Nature (London)* **421**, 539 (2003).  
 [5] C. M. Gray, A. K. Engel, P. Koenig, and W. Singer, *Eur. J. Neurosci.* **2**, 607 (1990).

- [6] J. U. Ramcharitar, E. W. Tan, and E. S. Fortune, *J. Neurophysiol.* **96**, 2319 (2006).
- [7] G. Buzsaki and A. Draguhn, *Science* **304**, 1926 (2004).
- [8] A. Angelucci, J. Levitt, E. Walton, J. Hupe, J. Bullier, and J. Lund, *J. Neurosci.* **22**, 8633 (2002).
- [9] J. Bullier, J. Hupe, A. James, and P. Girard, *Prog. Brain Res.* **134**, 193 (2001).
- [10] A. Angelucci and P. Bressloff, *Prog. Brain Res.* **154**, 93 (2006).
- [11] L. Schwabe, K. Obermayer, A. Angelucci, and P. C. Bressloff, *J. Neurosci.* **26**, 9117 (2006).
- [12] H. B. Barlow, *J. Opt. Technol.* **66**, 776 (1999).
- [13] A. Roxin, N. Brunel, and D. Hansel, *Phys. Rev. Lett.* **94**, 238103 (2005).
- [14] D. Hansel and H. Sompolinsky, *Phys. Rev. Lett.* **68**, 718 (1992).
- [15] M. Mattia and P. Del Giudice, *Phys. Rev. E* **66**, 051917 (2002).
- [16] N. Kopell and B. Ermentrout, *Proc. Natl. Acad. Sci. U.S.A.* **101**, 15482 (2004).
- [17] B. Doiron, B. Lindner, A. Longtin, L. Maler, and J. Bastian, *Phys. Rev. Lett.* **93**, 048101 (2004).
- [18] B. Lindner, B. Doiron, and A. Longtin, *Phys. Rev. E* **72**, 061919 (2005).
- [19] D. Marinazzo, H. J. Kappen, and S. C. A. M. Gielen, *Neural Comput.* **19**, 1739 (2007).
- [20] N. Masuda, B. Doiron, A. Longtin, and K. Aihara, *Neural Comput.* **17**, 2139 (2005).
- [21] M. J. Chacron, A. Longtin, and L. Maler, *Phys. Rev. E* **72**, 051917 (2005).
- [22] N. J. Berman and L. Maler, *J. Exp. Biol.* **202**, 1243 (1999).
- [23] D. Kleinfeld, E. Ahissar, and M. Diamond, *Curr. Opin. Neurobiol.* **16**, 435 (2006).
- [24] J. Chapin, J. Schneider, M. Nicolelis, and C. Lin, *Science* **248**, 1553 (1990).
- [25] S. Hamann, *Nat. Neurosci.* **8**, 701 (2005).
- [26] P. C. Bressloff and S. Coombes, *Int. J. Mod. Phys. B* **11**, 2343 (1997).
- [27] A. Hutt, M. Bestehorn, and T. Wennekers, *Network Comput. Neural Syst.* **14**, 351 (2003).
- [28] W. Freeman, *Neurodynamics: An Exploration in Mesoscopic Brain Dynamics (Perspectives in Neural Computing)* (Springer, Berlin, 2000).
- [29] P. Nunez and R. Srinivasan, *Electric Fields of the Brain: The Neurophysics of EEG* (Oxford University Press, New York, 2006).
- [30] A. Hutt and T. D. Frank, *Acta Phys. Pol. A* **108**, 1021 (2005).
- [31] C. Gardiner, *Handbook of Stochastic Methods* (Springer, Berlin, 2004).
- [32] J. Garcia-Ojalvo and J. Sancho, *Noise in Spatially Extended Systems* (Springer, New York, 1999).
- [33] C. Kayser and P. Koenig, *Eur. J. Neurosci.* **19**, 485 (2004).
- [34] B. Pesaran, J. Pezaris, M. Sahani, P. Mitra, and R. Andersen, *Nat. Neurosci.* **5**, 805 (2002).
- [35] N. Masuda, M. Okada, and K. Aihara, *Neural Comput.* **19**, 1854 (2007).